ELSEVIER

Spectrochimica Acta Part A xxx (2006) xxx–xxx

ACTA
PART A

www.elsevier.com/locate/saa

Novel Helmholtz-based photoacoustic sensor for trace gas detection at ppm level using GaInAsSb/GaAlAsSb DFB lasers

Mario Mattiello [a,*], Marc Niklès [a], Stéphane Schilt [b], Luc Thévenaz [b], Abdelmajid Salhi [c], David Barat [c], Aurore Vicet [c], Yves Rouillard [c], Ralph Werner [d], Johannes Koeth [d]

[a] *Omnisens SA, Science Park, CH-1015 Lausanne, Switzerland*
[b] *Ecole Polytechnique Fédérale de Lausanne (EPFL), Laboratory of Nanophotonics and Metrology (NAM), CH-1015 Lausanne, Switzerland*
[c] *Centre d'Electronique et de Microoptoélectronique de Montpellier (CEM2 UMR CNRS 5507), Université Montpellier II, F-34095 Montpellier Cedex 05, France*
[d] *Nanoplus Nanosystems and Technology GmbH, Oberer Kirschberg 4, D-97218 Gerbrunn, Germany*

Received 29 September 2005; received in revised form 1 November 2005; accepted 2 November 2005

Abstract

A new and compact photoacoustic sensor for trace gas detection in the 2–2.5 μm atmospheric window is reported. Both the development of antimonide-based DFB lasers with singlemode emission in this spectral range and a novel design of photoacoustic cell adapted to the characteristics of these lasers are discussed. The laser fabrication was made in two steps. The structure was firstly grown by molecular beam epitaxy then a metallic DFB grating was processed. The photoacoustic cell is based on a Helmholtz resonator that was designed in order to fully benefit from the highly divergent emission of the antimonide laser. An optimized modulation scheme based on wavelength modulation of the laser source combined with second harmonic detection has been implemented for efficient suppression of wall noise. Using a 2211 nm laser, sub-ppm detection limit has been demonstrated for ammonia.

Keywords: Photoacoustic spectroscopy; Antimonide; Semiconductor lasers; Trace gas monitoring; Helmholtz resonator

1. Introduction

Photoacoustic spectroscopy (PAS) has proven to be a very attractive technique for trace gas detection at parts-per-million (ppm) to parts-per-billion (ppb) range. It is based on sound generation in a gaseous sample resulting from absorption of a modulated laser beam. The detection of this sound using a sensitive microphone gives a linear response with respect to the effective concentration of the target gas. The major advantages of this method are a high sensitivity (down to sub-ppb level), a high linearity (over several orders of magnitude) and a wavelength-independent detection scheme, since acoustic detection is used instead of optical detection. This last feature makes this technique very well adapted for detection in the mid-infrared range, where photodetectors are costly and show poor performances, whereas mid-infrared is a very attractive spectral region for spectroscopy, since the absorption lines of most of the target gases (including CO, CH_4, NH_3 and HF) are one or two orders of magnitude stronger than in the near-infrared.

More particularly, the 2–2.5 μm range is very attractive for laser spectroscopy, since it is located in an atmospheric transmission window where absorption by water vapour and carbon dioxide is weak and where standard glass optical elements (windows, lenses) can still be used with reasonable losses. Therefore, the development of suitable laser sources in this spectral range for gas sensing is of great interest. The main important laser properties required for this type of applications are a single-mode emission and adequate spectral tunability in order to probe a single absorption line of the target species and to minimize the influence of interferents. When PAS is considered, optical power is another key parameter towards high sensitivity since photoacoustic (PA) signal linearly depends on the incident optical power. We report in this paper the development of DFB lasers in the 2–2.5 μm range and their application in trace gas sensing using PAS. Part of this work has been achieved in the frame of a European project including both laser manufacturers and sensors

* Corresponding author. Tel.: +41 21 693 56 04; fax: +41 21 693 26 14.
E-mail address: Mario.Mattiello@epfl.ch (M. Mattiello).

1386-1425/$ – see front matter © 2005 Elsevier B.V. All rights reserved.
doi:10.1016/j.saa.2005.11.006

designers. Antimonide-based semiconductor DFB lasers have been fabricated in a two-step process by CEM2 at University of Montpellier II (France) and Nanoplus (Germany). CEM2 made the growth of the laser structures and then Nanoplus processed a DFB grating to get singlemode emission. Later, these lasers were implemented in measuring systems for trace gas sensing using PAS by Omnisens in collaboration with EPFL (both in Switzerland). In order to benefit from the particular characteristics of these lasers, a novel PA cell based on a Helmholtz-resonator configuration has been developed and tested. Different gas species (CH_4, NH_3) have been probed at trace level using this novel PA cell and various DFB lasers developed at different wavelengths. Among these achievements, we report here sub-ppm detection limit for ammonia using the developed PA sensor in conjunction with a 2211 nm DFB laser developed for this purpose.

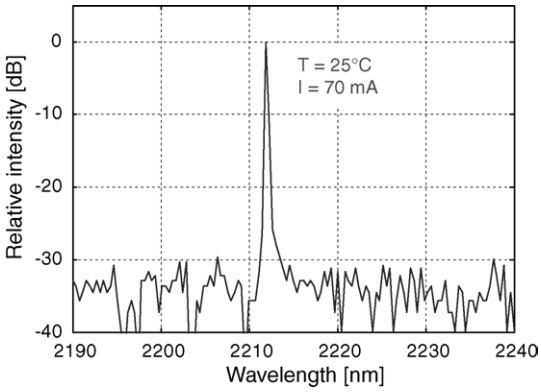

Fig. 2. Typical emission spectrum of an InGaAsSb/AlGaAsSb based quantum wells laser. Singlemode emission is demonstrated with a SMSR > 30 dB.

2. Antimonide-based DFB laser diodes

2.1. Lasers fabrication

The laser structures were grown at CEM2 by solid-source Molecular Beam Epitaxy (MBE). The MBE system used in Montpellier is a RIBER Compact 21E system equipped with two valved As and Sb cracker cells. The growth was carried out at 480 °C on a n-type GaSb substrate. Layers constituting the structures were grown in the following order (see Fig. 1): a 75 nm-thick n-type GaSb buffer, a 120 nm-thick n-layer graded from $Al_{0.10}Ga_{0.90}As_{0.03}Sb_{0.97}$ to $Al_{0.90}Ga_{0.10}As_{0.08}Sb_{0.92}$, a 1.5 μm-thick $Al_{0.90}Ga_{0.10}As_{0.08}Sb_{0.92}$ n-type (2×10^{18} cm^{-3}, Te) cladding layer, an undoped active zone consisting of three 10 nm-thick 1.6 % compressively strained QWs of $Ga_{0.65}In_{0.35}As_{0.08}Sb_{0.92}$ separated by two 35 nm-thick $Al_{0.25}Ga_{0.75}As_{0.02}Sb_{0.98}$ electronic barriers and enclosed between 375 nm-thick $Al_{0.25}Ga_{0.75}As_{0.02}Sb_{0.98}$ spacers, a 1.5 μm-thick p-type $Al_{0.90}Ga_{0.10}As_{0.08}Sb_{0.92}$ (5×10^{18} cm^{-3}, Be) cladding layer, a 120 nm-thick p-layer graded from $Al_{0.90}Ga_{0.10}As_{0.08}Sb_{0.92}$ to $Al_{0.10}Ga_{0.90}As_{0.03}Sb_{0.97}$ (1×10^{19} cm^{-3}, Be), and finally a 0.25 μm p$^+$-GaSb cap layer (Fig. 1). The p-doping level of the first 0.2 μm of the upper cladding near the active zone was decreased to 5×10^{17} cm^{-3} in order to reduce the inter-valence band absorption.

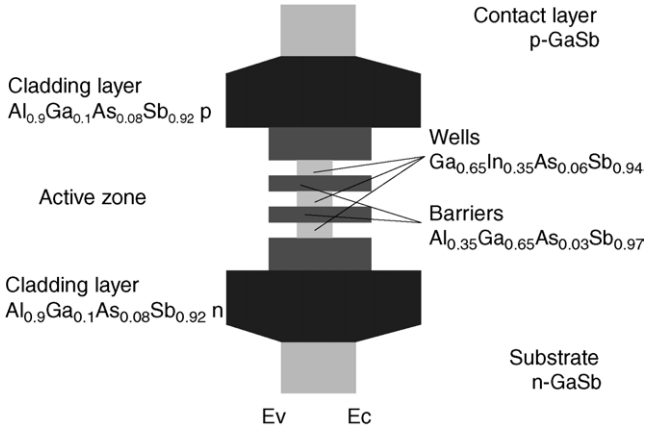

Fig. 1. Typical profile of the conduction and valence bands in the InGaAsSb/AlGaAsSb quantum wells lasers.

Standard technology for the fabrication of DFB laser diodes for optical telecommunication applications uses an etched grating buried within the laser structure. After an interruption of the growth of the layers the grating is structured using photolithography and wet- or dry-etching processes. After the etching the growth of the laser structure is finished. The need of an overgrowth after the grating process makes this technology very unsuitable for Aluminum containing material systems. Nanoplus has developed a technology that uses a lateral metal grating beside a ridge waveguide structure for the coupling between the light wave and the grating. The growth of the complete laser structure is finished in one step without any interruption before starting the DFB processing. After the epitaxy, a ridge waveguide structure is defined using lithography and transferred into the semiconductor surface by dry etching processes. In the next step, a metal grating is fabricated on both sides of the ridge using electron beam lithography and lift-off technology. The overlap of the lightwave with the metal lateral grating causes a single mode emission of the laser diode. According to the first order Bragg equation ($\lambda = \Lambda/2 \times n_{\text{eff}}$, with λ representing the emission wavelength, Λ the period of the lateral grating and n_{eff} the effective index of refraction of the laser structure) the emitting wavelength of the laser is directly related to the period of the lateral grating. Planarization of the ridge and metallization finish the laser process. A typical emission spectrum of a singlemode DFB laser diode fabricated with this technology is shown in Fig. 2. The spectrum was measured at room temperature in continuous wave (cw) operation mode using a grating spectrometer with 1150 mm focal length. The signal was detected by a PbS detector and lock-in amplifier. It is clearly seen that the emission spectra is singlemode and the side mode suppression ratio (SMSR) for this device is higher than 30 dB. In Fig. 3, the emission wavelength of a series of devices is plotted as a function of the grating period. Each of the devices has a slightly different grating period. By changing the grating period from 304.4 nm up to 306.68 nm, the wavelength of the DFB laser diodes can be shifted from 2209.15 nm to 2226.47 nm. This allows the realization of singlemode lasers over the complete gain region of the epitaxial wafer.

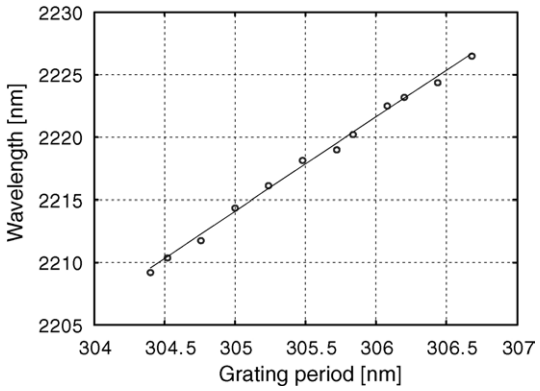

Fig. 3. Fine adjustment of the laser wavelength by DFB grating period change.

2.2. Lasers characterization

Among the various DFB lasers processed for different emission wavelengths, one laser emitting in the 2211-nm range has been selected in view of the realization of an ammonia sensor due to its coincidence with two rather strong NH_3 lines belonging to the $\nu_2 + \nu_3$ band.

A characterization of this DFB laser in terms of optical power and wavelength tunability has been performed. Laser power has been measured as a function of the injection current at different temperatures ranging from 15 °C to 40 °C using a thermal powermeter (Melles-Griot 13PEM001) directly mounted in front of the laser, without any collecting optics. The observed threshold current was in the range of 20–30 mA and the maximum measured optical power was 3.4 mW (at $T = 15$ °C and $I = 100$ mA), as shown in Fig. 4. This value was probably slightly underestimated due to an incomplete collection of the laser emission in our experimental set-up (due to the high divergence of the laser emission and to the limited aperture of the detector).

Laser wavelength and tuning coefficients were measured using a wavemeter (Burleigh WA-1000) with a picometer resolution. A nicely continuous tunability has been observed in the whole range of current and for temperatures from 20 °C to 40 °C as shown in Fig. 5. For lower temperatures, some mode hops occur for injection current below 80 mA. Typical tuning coefficients of −2 GHz/mA and −9 GHz/°C have been measured.

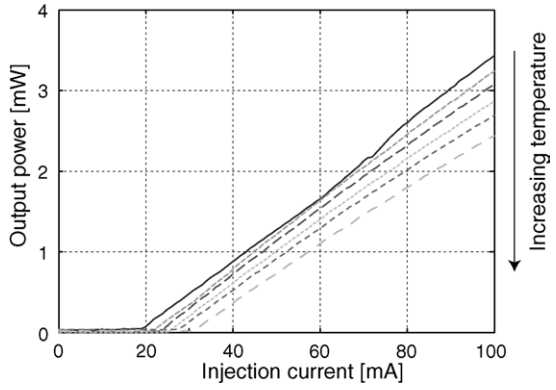

Fig. 4. *L–I* curves of a 2211 nm DFB laser measured at different temperatures (from 15 °C to 40 °C with 5 °C step).

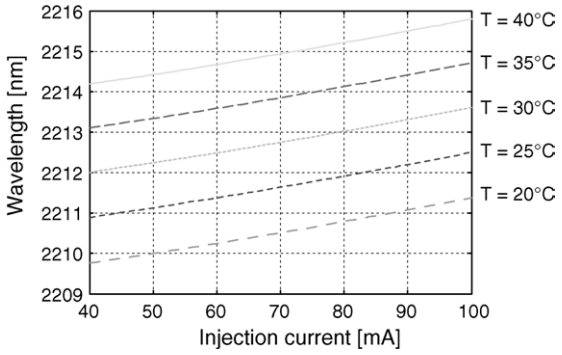

Fig. 5. Wavelength tunability of a 2211 nm DFB laser as a function of the injection current at different laser temperatures.

For all these measurements, the laser was mounted in a TO 5.6 windowless package and was temperature-stabilized using a commercial TE-cooled laser mount (Thorlabs TCLDM9).

3. Helmholtz-based photoacoustic spectroscopy

The developed DFB lasers have a largely divergent emission, as previously shown for a laser of the same type emitting at a slightly longer wavelength of 2372 nm for CH_4 sensing [1]. Typical divergence angles of 22° horizontally and 46° vertically (half angle at $1/e^2$) were obtained in that case. As a result of the high divergence of the laser, a poor efficiency is expected in the collection of the emitted optical power using collimating optics, thus resulting in large optical losses, extremely detrimental to PAS, since PA sensitivity directly depends on optical power. For this reason, a novel Helmholtz resonator configuration, which can positively exploit the divergence of the laser, has been designed and developed.

3.1. Theoretical background

A Helmholtz resonator is an acoustic system made of two volumes connected by a tube. When the acoustic wavelength is much larger than the resonator dimensions and the tube considerably small compared to the volumes, this resonant system behaves like a RLC electrical circuit, where the volumes correspond to capacitors and the tube to a resistance and an inductance in series as represented in Fig. 6. Such a circuit shows a resonance peak at the Helmholtz frequency:

$$f_0 = \frac{1}{2\pi\sqrt{L \cdot C_{\text{eq}}}} \tag{1}$$

where C_{eq} is an equivalent capacitor:

$$C_{\text{eq}} = \frac{C_1 \cdot C_2}{C_1 + C_2} \tag{2}$$

The quality factor of the resonance is given by:

$$Q = 2\pi f_0 \frac{L}{R} \tag{3}$$

Theory of acoustics establishes some mathematical expressions of the equivalent electrical parameters R, L and C as a func-

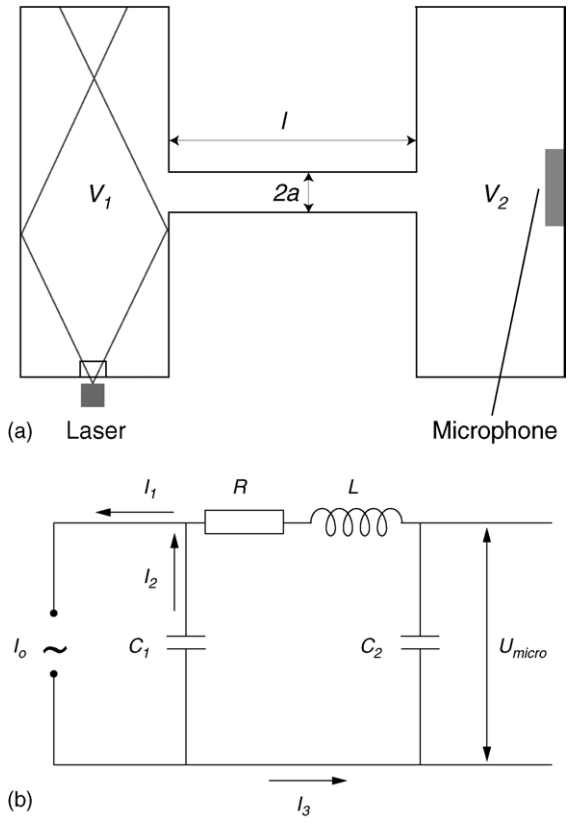

Fig. 6. (a) Schematic representation of a Helmholtz resonator. (b) Equivalent electrical circuit.

tion of the shape and dimensions of the corresponding acoustic elements. According to [2], the capacitors depend on the volume V_i, the air density ρ and the speed of sound c ($C_i = V_i/\rho c^2$), while the inductance and resistance are frequency-dependent and vary with respect to tube length l and radius a, to the air density ρ and viscosity η. Analytical expressions are obtained for L and R only in the two limit conditions where $r_v = a\sqrt{2\pi f\rho/\eta} < 1$ ($L = \rho l/\pi a^2$ and $R = 8\eta l/\pi a^4$) and $r_v > 100$ ($L = 4\rho l/\pi a^2$ and to $R = l\sqrt{4f\rho\eta/a^3}$). These relations, along with Kirchhoff's laws for electrical circuits, lead to the following theoretical expression for the so-called cell constant (i.e. the ratio between the PA signal generated in the cell and the absorbed optical power) at $f = f_0$:

$$C_{\text{cell}} = (\gamma - 1)\frac{\pi a^2 Q c^2}{l' V_1\ V_2 (2\pi f_0)^3} \tag{4}$$

where $\gamma = C_p/C_v$ is the ratio of the specific heat at constant pressure and constant volume, c the sound velocity, a the radius of the connecting tube, V_1 and V_2 the volumes and $l' = l + 1.7a$ the effective length of the connecting tube, i.e. the physical length l increased by a tube-end correction factor [3]. Eqs. (1), (3) and (4), together with the mathematical expressions established in [2], give the following dependence of the cell constant at $f = f_0$ as a function of its geometrical parameters in the case of a symmetrical resonator ($V_1 = V_2 = V$):

$$C_{\text{cell}} \propto a^{1/2} \cdot (l + 1.7a)^{1/4} \cdot V^{-3/4} \tag{5}$$

Hence, the cell efficiency is proportional to the tube dimensions and inversely proportional to the volumes size, so that small volumes and large tube lead to the best performances at first glance. However, the tube must be kept considerably smaller than the volumes in order to ensure correct Helmholtz resonator behaviour. Moreover, a certain number of geometrical and technical restrictions need to be respected. Physical conditions must be fulfilled to avoid the presence of acoustic eigenmodes, whereas technical considerations must be taken into account in order to make possible the positioning of different external elements, such as a microphone, a loud-speaker and gas inlet and outlet. Therefore, a trade-off on the cell dimensions has been found, taking into account all these conditions.

Since the acoustic wavelength is much larger than the cell dimensions, an important property of Helmholtz resonators is that the sound wave at a given time is approximately the same in each point of the resonator volumes, but is of opposite phase in the two volumes. In other words, the acoustic resonance does not depend on the location where the sound is either generated or measured, as it is the case for modal resonances, for which the sound magnitude depends on the overlap integral between the laser beam and the acoustic mode. In a Helmholtz resonator, the PA signal is independent from the laser beam geometry. This peculiarity makes Helmholtz resonators well adapted to be used with strongly divergent, non-collimated lasers. Moreover, a strong divergence, combined with high internal surface reflectivity, which may be obtained using gold-coated walls, increases the effective interaction length between light and gas, thus improving the PA sound generation. This configuration also offers the advantage to limit the number of optical elements to be used, thus reducing the optical power losses, leading to a simple, compact and efficient sensing scheme insensitive to alignment problems.

3.2. Novel compact Helmholtz-based PA cell

As the acoustic efficiency of a Helmholtz resonator is roughly inversely proportional to its size, the dimensions of the new cell have been made as small as possible. The final set-up includes a window and the gas inlet in the first volume and a microphone (Knowles EK-3132), a loud-speaker for acoustic resonance tracking (Kingstate KDM 13008-03) and the gas outlet in the other volume (see Fig. 7). The first volume of the resonator is illuminated by the divergent laser beam. In order to maximize the optical power launched into the cell, the laser is positioned as close as possible from the 1-mm thick cell window. The laser divergence is exploited by using multiple optical reflections on the volume internal surface, in order to increase the effective interaction length between light and gas. The efficiency of internal reflections is enhanced by depositing a gold coating on the cell walls. This gold coating is also expected to improve the response time of the cell for the measurement of polar molecules such as NH_3 that tends to stick to the cell walls, as gold is known to be an efficient material to reduce the adsorption/desorption effects [4].

Due to the very small size of the cell, each small parasitic volume (gas inlet/outlet, microphone, loud-speaker) has an influence on the acoustic response of the cell. To partially overcome

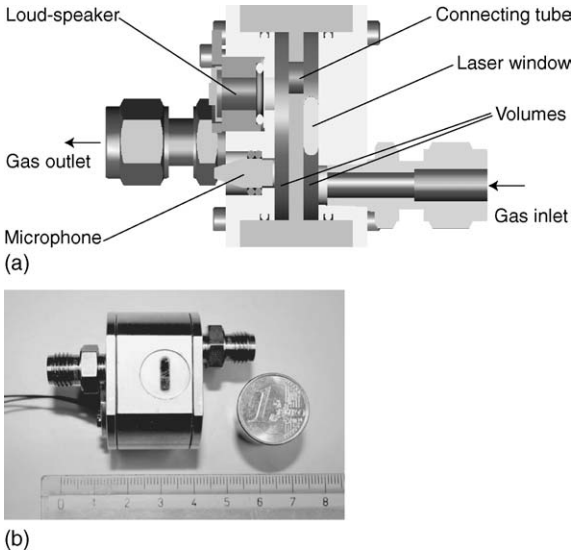

Fig. 7. (a) Schematic representation of the new photoacoustic cell. (b) Picture of the photoacoustic cell. The global size does not exceed 6 cm.

this issue, an acoustic "silencer" (made of a volume and a duct in series, the length of both being an odd multiple of a quarter of the acoustic wavelength in order to simulate an infinite acoustic impedance) has been added on both sides of the cell. Acoustic characterization of the cell has been performed by filling the cell with an absorbing gas and by exciting it using a laser of adequate wavelength. Fig. 8 displays the frequency response of the cell obtained using a 2372 nm DFB laser and CH_4 as an absorbing species. The Helmholtz resonance is observed at 2.6 kHz with a quality factor $Q \cong 25$, which is comparable to our knowledge to the best values reported in the literature for Helmholtz resonator used in PAS (see for example [5–7]). Similar performances have been obtained when exciting the resonance with a loud-speaker. The small resonance peaks observed at 1.8 kHz and 3.6 kHz are due to longitudinal resonance modes in the tubes and the volumes of the silencers, but they are far enough from the Helmholtz resonance not to affect the measurement.

The limiting factor of the simple geometry of our Helmholtz resonator that uses internal reflections in the excitation volume

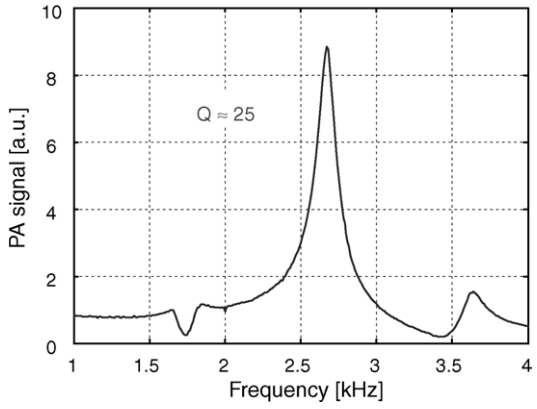

Fig. 8. Acoustic response of the novel PA cell measured using a 2372 nm DFB laser tuned to a CH_4 absorption line. The Helmholtz resonance is located at 2.6 kHz and has a quality factor around 25.

of the PA cell is associated to spurious wall noise that occurs as a result of light absorption by the cell walls. In this geometry, most of the light is eventually absorbed by the walls of the cell and not in the gas. As a result, walls are heated and also generate an acoustic wave at the laser modulation frequency. This parasitic sound acts as a noise that induces an offset in the measured acoustic signal and thus limits the sensitivity of the PA cell. One way to reduce the importance of this noise is to use appropriate wavelength modulation (WM) instead of intensity modulation (IM). Semiconductor lasers may be intensity- or wavelength-modulated depending on the laser modulation parameters, i.e. the operating current and modulation depth [8]. The use of WM enables to reduce the effect of wall noise, since wall absorption is wavelength-independent (on a narrow spectral range comparable to the width of a molecular absorption line) and is thus not able to induce an acoustic wave in case of pure laser WM. However, pure WM cannot be achieved when modulating the injection current of a semiconductor laser and residual IM is always present [9], which prevents a total suppression of wall noise. However, higher suppression rate may be achieved by combining WM and harmonic detection. In the WM-dominated regime, the generated PA signal is essentially proportional to the derivative of the target absorption line, whereas it is directly proportional to the absorption coefficient in the IM-dominated regime. Furthermore, nth harmonic detection may be performed with WM, which gives rise to a *n*th derivative of the absorption line. Since IM essentially occurs at the fundamental modulation frequency in a semiconductor laser, second harmonic (2*f*) detection enables to efficiently suppress wall noise, while maintaining a strong PA signal. Practically, 2*f*-PAS has been implemented by modulating the laser current at half the Helmholtz frequency, so that 2*f*-PA signal has been generated at the Helmholtz frequency in order to benefit from the resonator amplification. The efficiency of wall noise suppression using this modulation scheme is illustrated in Fig. 9, which shows a comparison between the response of the PA cell for 1*f* and 2*f* detection. These results were obtained in a preliminary characterization of the cell performed with a 2372 nm DFB laser used for CH_4 sensing [1]. A very large offset is observed in the PA signal in absence of CH_4 for 1*f* detection, whereas an offset-free signal is obtained with 2*f* detection. As a result of these observations, WM with 2*f* detection was then always used, in particular for ammonia sensing at 2211 nm.

3.3. Ammonia sensing

As shown in Section 2.2, the DFB laser used for NH_3 sensing can be continuously tuned between 2210 nm and 2215 nm. In this range, several absorption lines of ammonia have been measured and identified as shown in Fig. 10. The PA spectrum of ammonia has been measured in this case using laser IM and 1*f* detection, in order to enable easy comparison with the spectrum calculated from Hitran database [10]. The large offset observed in the experimental spectrum is induced by wall noise as discussed in Section 3.2. Among these lines, the two strongest are located at, respectively, 2211.2 nm and 2213.9 nm. The assignment of these lines is *arR*(6,9) and *arR*(4,0), respectively. The former

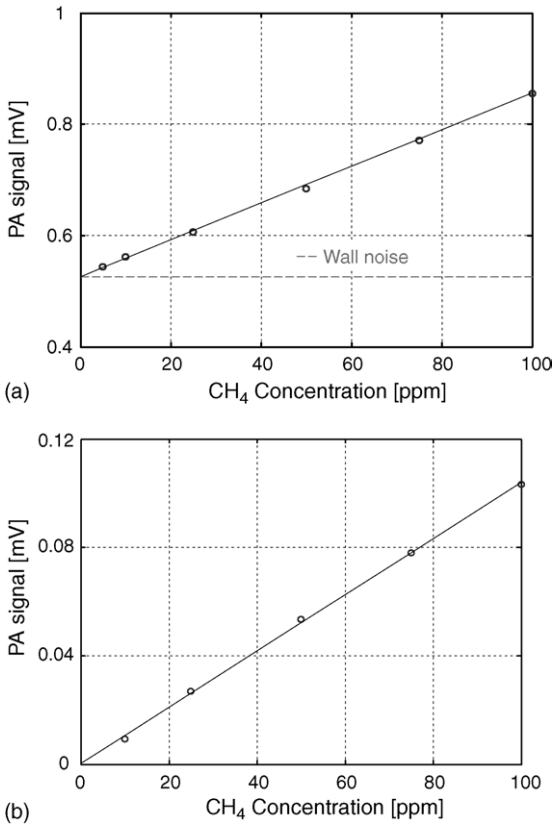

Fig. 9. Experimental demonstration of the efficiency of wall noise suppression in the PA cell by combining wavelength modulation with 2*f* detection (b) compared to 1*f* detection (a). The amplitude of the measured acoustic signal is displayed as a function of the CH_4 concentration when the PA cell was illuminating using a 2372 nm DFB laser tuned to an absorption line of methane.

has a slightly lower absorption coefficient (0.55 cm^{-1} versus 0.63 cm^{-1} at atmospheric pressure), but this line can be reached at a lower laser temperature (for the same injection current), thus with an optical power approximately 20% higher compared to the latter. As the PA signal linearly depends on optical power, ammonia detection has been performed at 2211.2 nm.

A typical 2*f* PA signal obtained by scanning the laser through the NH_3 line (by varying the laser temperature) is shown in

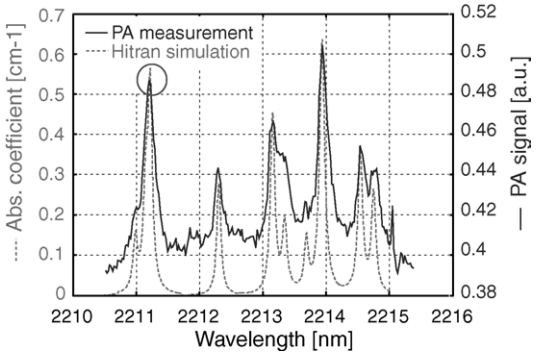

Fig. 10. Absorption spectrum of ammonia in the 2209–2215 nm range. The dashed curve represents the spectrum calculated from Hitran database, whereas the solid curve is the measured PA signal corresponding to 100 ppm of NH_3. The circle shows the absorption line used for ammonia sensing.

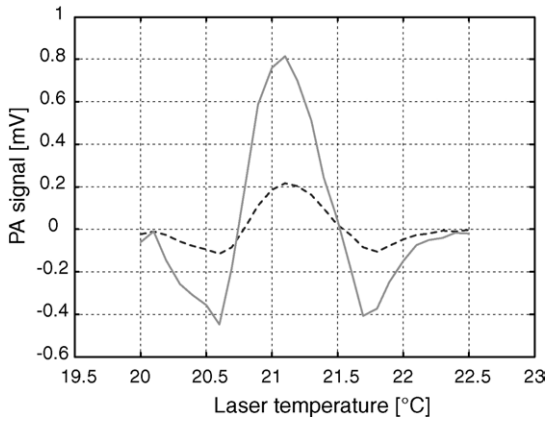

Fig. 11. 2*f* PA signal of the *arR*(6,9) line of ammonia at 2211.2 nm. The measurement has been performed by scanning the laser temperature. A typical second derivative of the absorption line is obtained. The positive effect of the cell internal gold coating is demonstrated by comparing the signals obtained in an uncoated stainless steel cell (dashed line) and in a gold-coated cell (solid line), showing an enhancement by a factor of four.

Fig. 11. A second derivative of the absorption line is obtained, as expected. The positive effect of the cell internal gold coating is also demonstrated and an enhancement of the PA signal by a factor of four has been measured with the gold-coated cell compared to the original stainless steel PA cell. This improvement mainly results from the higher surface reflectivity provided by the gold coating, which increases the interaction length between light and gas.

A multi-gas controlling unit (MKS 647C) with mass flow controllers (MKS 1179) has been used to generate different concentrations of NH_3 from a certified cylinder of 100 ppm buffered in nitrogen. The PA signal has been measured for each concentration and results are displayed in Fig. 12. Excellent linearity ($R^2 > 0.99$) has been obtained with a detection limit (defined for a signal-to-noise ratio SNR = 3) of 0.5 ppm for an integration time of 10 s. The experimental cell constant C_{exp} is defined as:

$$C_{exp} = \frac{U}{M\alpha P_o C}, \quad (6)$$

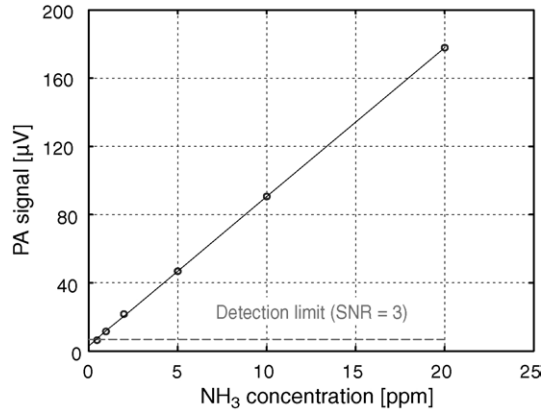

Fig. 12. Sensor response as a function of ammonia concentration. The dots represent experimental data, the line is a linear fit and the dashed line represents the detection limit, defined for a signal-to-noise ratio SNR = 3 and an integration time of 10 s. The detection limit corresponds to 0.5 ppm of NH_3.

where U is the measured photoacoustic signal, M the microphone sensitivity (in [V/Pa]), α the absorption coefficient of the target gas, P_o the average optical power and C is the gas concentration. A value $C_{exp} = 660$ [Pa W^{-1} cm] is obtained for our Helmholtz-based PA cell. This is approximately one order of magnitude smaller than the value reported for the differential Helmholtz resonator from Zéninari et al. [5], which may be explained by the 10-fold higher operation frequency of our cell, since the cell constant varies as $1/f^2$ according to Eqs. (3) and (4). However, the higher resonant frequency of our cell offers other advantages, such as in term of immunity to ambient acoustic noise.

4. Conclusion

Antimonide-based DFB laser have been produced in a wide spectral range in the 2–2.5 μm atmospheric window. These lasers present all the required properties for high resolution gas sensing applications, such as singlemode emission with >30 dB SMSR and continuous tunability over several nanometers. The tunability enables precise adjustment of the laser wavelength to a molecular absorption line and can also provide possibilities to perform multi-gas detection by sequentially addressing different absorption lines.

Regarding PAS applications, these lasers deliver an optical power limited to a few mW and their large divergence makes difficult an efficient collection of the emitted power. For these reasons, a novel PA cell has been developed and tested with the objective to exploit this divergence. This cell is based on a Helmholtz resonator, in which the divergent laser emission directly illuminates one of the volumes of the resonator and multiple optical reflections are fully exploited to increase the effective interaction length between light and gas. An enhancement of the PA signal by a factor of four has been achieved by gold deposition in the cell in order to reinforce the reflections. An efficient modulation scheme based on WM with 2f detection has been implemented in order to suppress wall noise, leading to very low zero-offset and allowing sub-ppm measurements. Finally, a sub-ppm detection limit (0.5 ppm for a signal-to-noise ratio SNR = 3) for NH_3 at 2211 nm with only 3 mW of optical power has been demonstrated.

The developed detection system presents important competitive advantages in terms of size and robustness. In addition to being quite simple, the cell design does not include any moving parts, requires very simple and uncritical optical alignment that guarantees robustness and long term stable operation. The cell design is also totally compatible with any semiconductor laser, without any required collecting or collimating optics, in opposition to the other photoacoustic systems. In addition, this cell design represents an attractive solution for the implementation of PAS with quantum-cascade lasers (QCL) in the mid-infrared, since these laser sources also suffer from a highly divergent emission that is extremely difficult to be efficiently collected.

Acknowledgments

This work has been partly supported by the European Community through the GLADIS contract (IST-2001-35178).

The authors from Montpellier are also grateful to the Languedoc-Roussillon Region for its support.

Authors from EPFL are grateful to Omnisens SA for supporting this research.

References

[1] S. Schilt, A. Vicet, R. Werner, M. Mattiello, L. Thevenaz, A. Salhi, Y. Rouillard, J. Koeth, Spectrochim. Acta A 60 (2003) 3431–3436.
[2] A.H. Benade, J. Acoust. Soc. Am. 22 (1968) 616–623.
[3] D.T. Blackstock, Fundamentals of Physical Acoustics, Wiley, 2000, 151–152.
[4] S.M. Beck, Appl. Opt. 24 (1985) 1761–1763.
[5] V. Zéninari, V.A. Kapitanov, D. Courtois, Yu.N. Ponomarev, Infrared Phys. Technol. 40 (1999) 1–23.
[6] R. Kästle, M.W. Sigrist, Appl. Phys. B 63 (1996) 389–397.
[7] S. Barbieri, J.-P. Pellaux, E. Studemann, D. Rosset, Rev. Sci. Instrum. 73 (2002) 2458–2461.
[8] S. Schilt, L. Thévenaz, Infrared Phys. Technol., in press, doi:10.1016/j.infrared.2005.09.001.
[9] S. Schilt, L. Thévenaz, P. Robert, Appl. Opt. 42 (2003) 6728–6738.
[10] L.S. Rothman, D. Jacquemart, A. Barbe, D. Chris Benner, M. Birk, L.R. Brown, M.R. Carleer, C. Chackerian Jr., K. Chance, et al., J. Quant. Spectrosc. Radiat. Transfer 96 (2) (2005) 139–204.